Dalton Transactions

ROYAL SOCIETY OF CHEMISTRY

PAPER

View Article Online
View Journal | View Issue

Cite this: *Dalton Trans.*, 2020, **49**, 1854

NLO-active Y-shaped ferrocene conjugated imidazole chromophores as precursors for SHG polymeric films†

Selvam Prabu, [a] Ezhumalai David, [a] Thamodharan Viswanathan, [a] Krishnan Thirumoorthy, [a] Tamas Panda,[a] Claudia Dragonetti, *[b,c] Alessia Colombo, [b,c] Daniele Marinotto,[b,c] Stefania Righetto,[b] Dominique Roberto [b,c] and Nallasamy Palanisami *[a]

Received 11th September 2019,
Accepted 8th January 2020

DOI: 10.1039/c9dt03637g

rsc.li/dalton

New Y-shaped ferrocene conjugated imidazole chromophores were prepared and fully characterized. The Y-shaped structure was confirmed by the single crystal X-ray diffraction technique. The chromophores show interesting second-order nonlinear optical (NLO) properties in solution, as determined by the Electric-Field Induced Second Harmonic generation (EFISH) technique. Remarkably, the trifluoro substituted compound **3** is characterized by a high $\mu\beta_{EFISH}$ value and has good potential as a molecular building block for composite films with Second Harmonic Generation (SHG) properties. For all compounds, the dipole moments and frontier orbital energies were calculated by the Density Functional Theoretical method.

Introduction

The development of second-order nonlinear optical (NLO) chromophores is an exciting proposition with emerging applications in electro-optic modulators, optical data storage devices, telecommunications and optical switches.[1] In particular, organic chromophores containing a donor–π-acceptor system show effective intramolecular charge transfer (ICT) from a donor to an acceptor, leading to a dipolar push–pull structure featuring low-energy and intense CT absorptions.[2] The polarizability and the linear and nonlinear optical properties of these systems depend on their chemical structure, the electronic behaviour of the appended donors and acceptors, and the length of the π-conjugated linker.[3] Extraordinary arrangements of peculiar chromophores, inspired by the letters of the alphabet (H, L, T, V, X, and Y), have appeared recently in the literature.[4] These chromophores, characterized by surprising photophysical properties, have been expediently utilized in organic light-emitting diodes (OLEDs),[5a] two-photon absorbers (2PAs),[5b] near-infrared absorbing dyes,[5c] dye-sensitized solar cells (DSSCs)[5d] and bulk-heterojunction solar cells (BHJSCs).[5e,f]

Besides, it is known that metal complexes provide several advantages over organic molecules in the field of second-order nonlinear optics due to their additional flexibility, thanks to the presence of the NLO active electronic charge-transfer transitions between the metals and the ligands, which are tuneable by virtue of the nature, oxidation state and coordination sphere of the metal centres.[6]

The use of heteroaromatic scaffolds, as π-backbones in NLO-active chromophores, provides high chemical and thermal robustness. In addition, they may act as auxiliary donors or acceptors, improving the optical nonlinearity of the chromophores.[7] Among them, imidazole moieties have been incorporated in chromophore systems as strong electron acceptors because of their high electron deficiency originating from two asymmetric nitrogen atoms that lower the π* level of the conjugated system.[8]

Push–pull Y-shaped imidazole (IM) chromophores of the type [(D–π)$_2$–IM–π–A], where two donors are at the peripheral (C4/C5) positions of imidazole and one acceptor at the C2 position, are characterized by a high charge transferability due to the presence of electron deficient nitrogen in the imidazole unit.[9] Some reports are available in the literature based on organic Y-shaped imidazole chromophores for NLO,[10] organic light-emitting diodes (OLEDs)[5a] and two-photon absorbers,[5b] but the NLO properties of organometallic Y-shaped imidazole systems have not been reported until now.

[a]*Department of Chemistry, School of Advanced Science, Vellore Institute of Technology, Vellore 632014, Tamilnadu, India. E-mail: palanisami.n@gmail.com; Tel: +91 98426 39776*
[b]*Department of Chemistry and Centro CIMAINA, University of Milan, INSTM-Research Unit, Via C. Golgi 19, 20133, Italy.*
E-mail: claudia.dragonetti@unimi.it
[c]*ISTM-CNR, via Golgi 19, Milan, Italy*

†Electronic supplementary information (ESI) available: X-ray crystallographic data, and all experimental details. CCDC 1885673. For ESI and crystallographic data in CIF or other electronic format see DOI: 10.1039/C9DT03637G

Ferrocene chromophores have been explored in the field of NLO and they have played the crucial role of an electron-donor in charge transfer processes, when ferrocene is linked to an acceptor moiety in push–pull molecules.[6d,11] A ferrocene complex was the first organometallic species reported in second-order nonlinear optics (NLO); it was described as a donor moiety by Green *et al.*[12a] Later, ferrocene based second-order NLO chromophores of the type D–π–A with different acceptor units such as heteroarenes,[12b] metal carbonyls,[12c] porphyrinoids[12d] and heteroaromatic[12e] acceptors were reported, with an increase in the electron-withdrawing strength of the acceptor and in the length of the π-delocalized bridge between the donor and the acceptor groups, in turn, leading to an increase in the β values.[12] Even though ferrocene-containing Y-shaped imidazole chromophores, described by Nair *et al.*, show great potential as multichannel ditopic chemosensors for biologically active cations/anions and the oxidative cleavage of DNA in the presence of H_2O_2,[13] to our knowledge their NLO properties have not been reported yet. The Y-shaped organometallic chromophore enables good coupling between the d orbitals of the metal and the π* system of the imidazole moiety, which could afford a substantial NLO response controlled by metal-to-ligand charge transfer transitions (MLCTs). Recently some of us have explored Y-shaped biferrocenyl quinoxaline donor-π-acceptor based chromophores, placing in evidence their high second-order NLO response in solution, as determined by the Electric Field Induced Second Harmonic (EFISH) technique. The dispersion of this kind of chromophore as a guest in a polymethylmethacrylate matrix (PMMA) can lead to the formation of a composite film with a good SHG response.[14]

Inspired by the aforementioned considerations, we have synthesized Y-shaped imidazole chromophores and fully characterized them with the aid of analytical and spectroscopic techniques such as FT-IR, ^{1}H, ^{13}C, ^{19}F NMR and elemental analysis. The structure has been analyzed by the single crystal X-ray diffraction (XRD) technique and the electrochemical behavior of the chromophores was investigated by cyclic voltammetry. The second-order non-linear optical properties were examined by the EFISH generation technique.

Results and discussion

Synthesis and characterization

Y-shaped imidazole chromophores **1–5** were synthesized by the Debus–Radziszewski condensation of 1,6-bis-ferrocenylhexa-1,5-diene-3,4-dione with a *para*-substituted benzaldehyde to yield imidazole derivatives as shown in Scheme 1.

The ^{1}H, ^{13}C, and ^{19}F (compound **3**) NMR spectra of chromophores **1–5** were measured in DMSO-d_6 at room temperature and the spectra are shown in Fig. S2–S12.† In the ^{1}H NMR spectra of chromophores **1–5**, the ferrocene protons appear at 4.1–4.6 ppm. The aliphatic CH protons are resonating at 6.9–7.1 ppm as two overlapping doublets and the –NH protons are at 12.2 ppm as a singlet. In the ^{13}C NMR spectra of

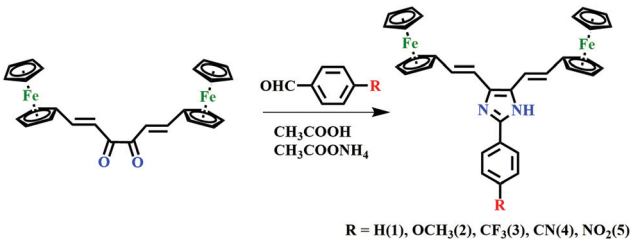

Scheme 1 Synthetic routes for different substituted Y-shaped imidazole chromophores.

chromophores **1–5**, the ferrocene carbons resonate at 69.24–79.73 ppm and the –C≡N carbon of compound **4** resonates at 119.4 ppm. The phenyl group carbons appear in the expected regions. The ^{19}F NMR spectrum of CF_3 (compound **3**) shows a signal at −60.8 ppm. The mass spectra of chromophores **1–5**, shown in Fig. S15–S19,† are in agreement with the theoretical mass. In addition, the thermal stability of Y-shaped molecules **1** and **4** was examined by thermogravimetric analysis (TGA) at a heating rate of 20 °C min^{-1} up to 800 °C, placing in evidence that the molecules are stable up to 320 °C (Fig. S13†). The Y-shaped structure of compound **4** was confirmed by the single crystal X-ray diffraction (XRD) method. Compound **4** was recrystallized from methanol at room temperature and the structure is shown in Fig. 1. The data collections, structure refinement and the parametric data of the unit cells are given in Table S1.† The single crystal structure of chromophore **4** revealed that the molecule has a Y-shaped structure, in which two ferrocenes lie above and below the plane leading to an antennae type structure. In addition, we observed H-bonding between the acidic –N–H proton of imidazole and the oxygen of a methanol molecule (H···O), as

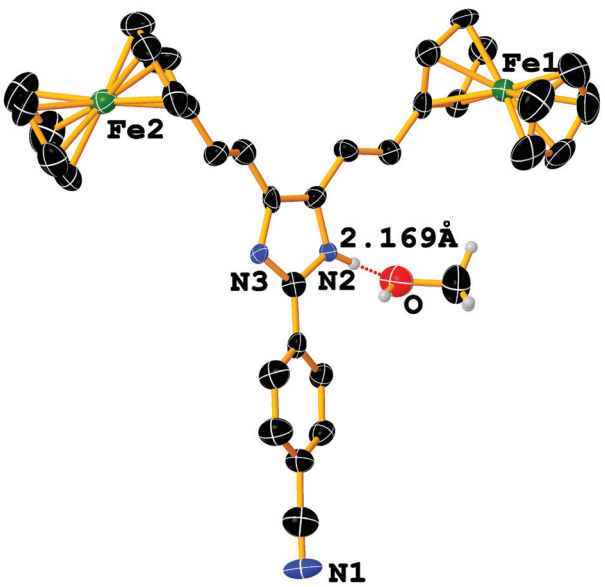

Fig. 1 Single crystal X-ray structure of compound **4**; hydrogen atoms are omitted for clarity.

shown in Fig. 1. The two cyclopentadienyl rings of ferrocene are in a staggered conformation with a torsion angle of 36°.[15] The data obtained with density functional theory (DFT) is correlated with the X-ray analysis of chromophore **4**, which is provided in the ESI.†

Electronic absorption spectra

The electronic absorption spectra of chromophores **1–5**, recorded in dichloromethane solution, show variable intense charge transfer absorptions (Fig. 2). In these spectra, we observed a higher energy band at 233–235 nm, originating from the ligand centred π–π* electronic transition and most intense n–π* electronic transition peaks in the range of 367–372 nm due to either metal-to-ligand charge transfer (MLCT) or ligand-to-metal charge transfer (LMCT) caused by intramolecular charge transfer (ICT). Theoretically calculated higher energy (HE) absorption bands for compounds **1–5** are in the range of 360–404 nm. There are other weak absorption bands of lower energy (469–495 nm), observed experimentally, which can be attributed to the d–d transition (assigned to $^1E_{1g} \leftarrow {}^1A_{1g}$) or metal-to-ligand charge transfer (dπ–π*) between Fe(II) and the cyclopentadienyl ring.[16] The absorptions and their energy gaps are shown in Table 1.

Electrochemical studies

The electrochemical behaviour of chromophores **1–5** was explored through cyclic voltammetry in dichloromethane solution containing 0.1 M tetrabutylammonium perchlorate (TBAP) as a supporting electrolyte at a scan rate of 100 mV s^{-1}. The counter electrode was a platinum wire, glassy carbon was used as the working electrode, and an Ag/AgCl electrode was used as the reference electrode.[16b,c] The cyclic voltammograms of the chromophores are shown in Fig. 3. Compounds **1–5** exhibit quasi-reversibility and a current ratio (i_{pa}/i_{pc}) equal to unity in the electrochemical assessment. The oxidation process of the ferrocenyl ($Fe^{2+} \rightleftharpoons Fe^{3+}$) core within the potential range from 0.42 to +0.61 V is related to the presence of donor/acceptor moieties. The oxidation potential of free ferrocene was +0.40 V under the same experimental conditions.[17] The half-wave potential, calculated by $E_{1/2} = (E_{pa} + E_{pc})/2$, of the novel compounds is more positive due to the *para*-substitution effect, as shown in Fig. 3. The potential of compound **2** was shifted to the right side due to the presence of a donor group ($-OCH_3$). The electrochemical data for these chromophores are summarized in Table S2.† The electrochemical potential of the compounds provides information about the HOMO and

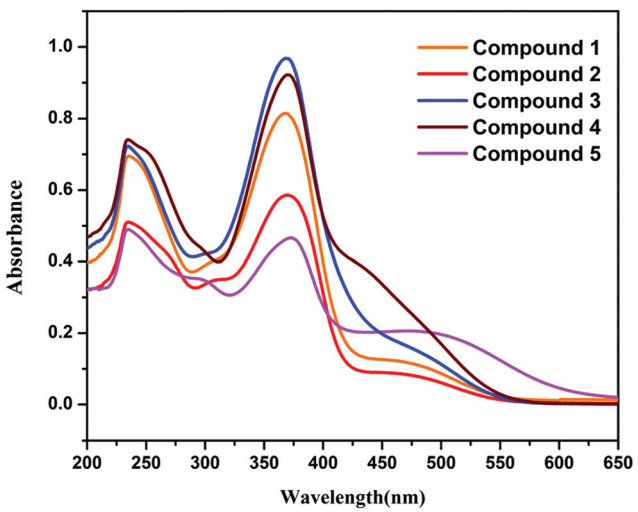

Fig. 2 Absorption spectra of compounds **1–5** in CH_2Cl_2 solution (1 × 10^{-5} M).

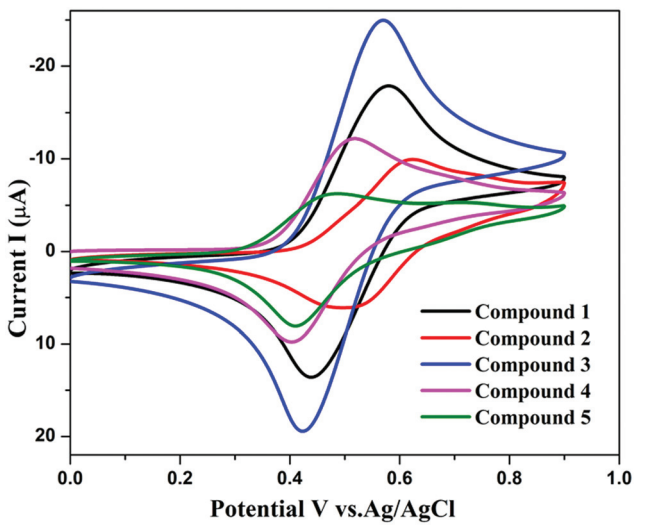

Fig. 3 Cyclic voltammograms of compounds **1–5** in the presence of a 0.1 M TBAP supporting electrolyte at 0.1 mV s^{-1} in 10^{-3} M CH_2Cl_2 solution.

Table 1 Photophysical and second order NLO properties of compounds **1–5**

Chromophore	λ_{max}^{ME} [a] [nm/(eV)] ε^a ($\times 10^5$) [M^{-1} cm^{-1}]	λ_{max}^{LE} [a] [nm/(eV)] ε^a ($\times 10^5$) [M^{-1} cm^{-1}]	HOMO[b] (eV)	LUMO[b] (eV)	λ_{max} [b] [nm (eV)]	μ_{gas}/μ_{DCM} [b] ($\times 10^{-18}$ esu)	$\mu\beta_{EFISH}$ [c] ($\times 10^{-48}$ esu)	β_{EFISH} [d] ($\times 10^{-30}$ esu)
Compound **1**	367(3.37)/0.81	469(2.64)/0.12	−4.91	−1.68	380 (3.25)	2.7/3.1	−415	−134
Compound **2**	370(3.35)/0.58	470(2.63)/0.08	−4.81	−1.57	382 (3.23)	4.1/4.2	−436	−104
Compound **3**	371(3.34)/0.92	460(2.69)/0.35	−5.09	−2.04	401 (3.08)	5.1/5.6	−1000	−179
Compound **4**	370(3.35)/0.96	438(2.83)/0.19	−5.15	−2.29	360 (3.44)	7.0/7.3	−970	−133
Compound **5**	372(3.33)/0.46	480(2.58)/0.19	−5.21	−2.95	404 (3.06)	8.0/8.1	−900	−111

[a] Experimental data (HE = high energy, ME = medium energy, and LE = low energy). [b] Theoretical calculations with TD-DFT. [c] In anhydrous $CHCl_3$, the estimated uncertainty in EFISH measurements is 10%. [d] β_{EFISH} was calculated using the computed μ_{DCM} value.

LUMO energy levels, $E_{HOMO} = -e\ (E_{ox} + 4.4)$ and $E_{LUMO} = (E_g^{optical} + E_{HOMO})$ respectively.[16c,18]

DFT studies

To optimize the molecular structures of the Y-shaped compounds **1–5**, we have carried out DFT computations using the B3LYP[19] method with the 6-31+G** basis set. The selected optimized geometrical parameters, calculated highest occupied molecular orbital (HOMO) and lowest unoccupied molecular orbital (LUMO) energies and absorption maxima (λ_{max}), are reported in Table 1. Based on the computed results, it is clear that the HOMO and LUMO distribution developed through the charge exchange from the bi-ferrocenyl donor and imidazole to the acceptor unit. In compounds **1–5**, the HOMO is mainly localized on the ferrocene moiety and the π-spacer double bond along with a part of the imidazole unit. Compounds **3**, **4** and **5** show slight stabilization when compared with **1** and **2**. The calculated HOMO energy level of compounds **1** and **2** varies from −4.80 eV to −5.21 eV. The LUMO energy level of compounds **3–5** is strongly stabilized when compared to **1** and **2**. The LUMO is localized in part on the imidazole unit and on the acceptor group present at the *para*-position of the aromatic ring as shown in Fig. 4. Here, we noticed that the imidazole ring participates in the HOMO and in LUMO levels and it contributes to the balanced charge transfer in compounds **1–5**.[20] Furthermore, we have performed time-dependent density functional theory (TD-DFT) calculations for compounds **1–5** to assign the definite transition observed in the experiments (Table 1). They provide evidence for the experimental red shift of the HE bands observed by increasing the electron accepting nature of the substituent present at the *para*-position of the aromatic ring. Compounds **1–5** make major contributions (more than 50%) to the relatively strong higher energy (HE) band $S_0 \rightarrow S_1$ transitions, indicating the intramolecular charge transfer (ICT) character of the HE band. For compounds **1–3**, the major contribution to the HE band is the HOMO → LUMO transitions whereas for **4** and **5** the major contribution to the HE band is the HOMO → LUMO+1 transition. The electronic structures, excited state energies, oscillator strengths and orbital transitions of compounds **1–5** are given in Tables S3 and S4.†

Second-order nonlinear optical properties

The electric field induced second harmonic (EFISH) generation technique[21] was used to determine the second-order nonlinear optical properties of the novel Y-shaped chromophores, in $CHCl_3$ at 10^{-3} M concentration with a non-resonant incident wavelength of 1.907 μm, obtained by Raman-shifting under high hydrogen pressure by using a Q-switched, mode-locked Nd^{3+}:YAG laser. This method is one of the valuable alternatives to Hyper-Rayleigh Scattering (HRS),[22] which suffers from the restriction of possible overestimation of the values of quadratic hyperpolarizability due to multi-photon fluorescence. EFISH measurements can provide direct

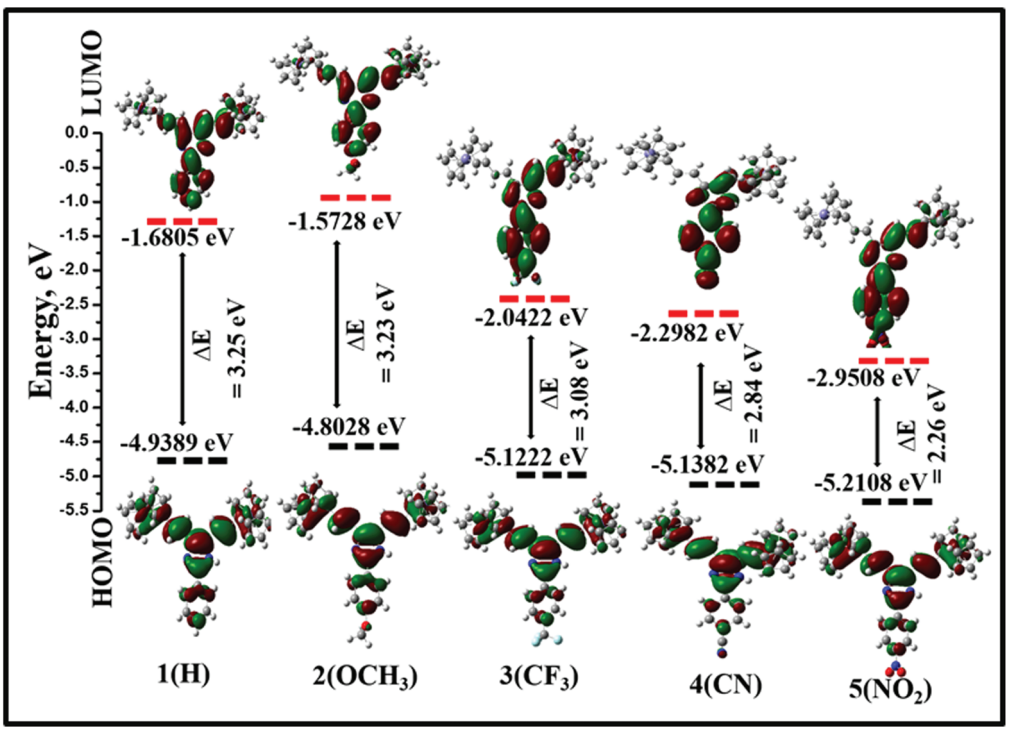

Fig. 4 Schematic orbital energy levels of chromophores **1–5** at the B3LYP/6-31+G** level of theory in a solvent phase (CH_2Cl_2). The energy gaps and orbital distribution of HOMO and LUMO are also shown.

information on the intrinsic molecular NLO properties through eqn (1)

$$\gamma_{\mathrm{EFISH}} = (\mu\beta_{\lambda}/5kT) + \gamma(-2\omega;\ \omega;\ \omega;\ 0) \quad (1)$$

where $\mu\beta\lambda/5kT$ is the dipolar orientational contribution of non-linearity to the molecule, and γ $(-2\omega, \omega, \omega, 0)$, the third order polarizability at frequency ω of the incident light, is a purely electronic cubic contribution to γ_{EFISH} which can usually be ignored, when studying the second-order NLO properties of dipolar molecules. Chromophores **1–5** show good $\mu\beta_{\mathrm{EFISH}}$ values (−415 to −1000 × 10^{-48} esu), remarkably as high as those previously observed for other Y-shaped ferrocenyl quinoxaline chromophores[14f] (Table 1). A similar high second-order NLO response was observed for other ferrocene chromophores.[12] Compounds **3–5** show high $\mu\beta_{\mathrm{EFISH}}$ due to the electron acceptor group present at the *para*-position of the aromatic ring. In addition, compound **3** shows the highest $\mu\beta_{\mathrm{EFISH}}$ value among the investigated compounds, because the CF_3 moiety has a low-lying n–π* excited state which favors the charge transfer process.[23] Also, TD-DFT studies of compound **3** show a high oscillator strength with low transition energy, which is in agreement with the particular high β value.[24]

To evaluate the quadratic hyperpolarizability (β_{EFISH}) of the chromophores, it is necessary to know the dipole moment (μ). Here, we have calculated a theoretical dipole moment in the gas phase and solvent phase (CH_2Cl_2) for compounds **1–5** with the B3LYP/6-31+G** level of theory. Similar values were obtained in both gas and solvent phases, indicating that there are no significant solute–solvent interactions. The acceptor groups in compounds **3–5** lead to a relatively high dipole moment, as shown in Table 1, following the same trend of the $\mu\beta_{\mathrm{EFISH}}$ values. We observed good β_{EFISH} values (−134, −104, −179, −133 and −111 × 10^{-30} esu for compounds **1**, **2**, **3**, **4**, and **5** respectively). The lowest quadratic hyperpolarizability was observed in the presence of the OCH_3 donor group (**2**) whereas the best value was achieved with compound **3**.

Some of us have the experience in the study of the second harmonic generation (SHG) signal of poled host–guest systems;[14] in particular, we have recently reported PMMA (polymethylmethacrylate) and PS (polystyrene) films containing a ferrocene conjugated quinoxaline chromophore which have shown remarkably high and stable SHG.[14f]

The high $\mu\beta_{\mathrm{EFISH}}$ value of compound **3** prompted us to explore its potential as a molecular building block for a composite thin film with SHG properties. It was dispersed in PMMA matrices (5 wt% of chromophores with respect to the matrix) and oriented by poling (ESI†). The corona wire poling dynamics of the SHG behaviour of the PMMA composite thin film is reported in Fig. 5. The electronic absorption spectra of compound **3** in the PMMA film before and after poling are reported in Fig. S1.† After poling, the film showed an absorption band intensity which was about 83% of that observed before poling. This decrease in the absorption peak intensity, called the dichroic effect,[25] is due to the partial orientation of the molecules along the direction of the electric poling field.

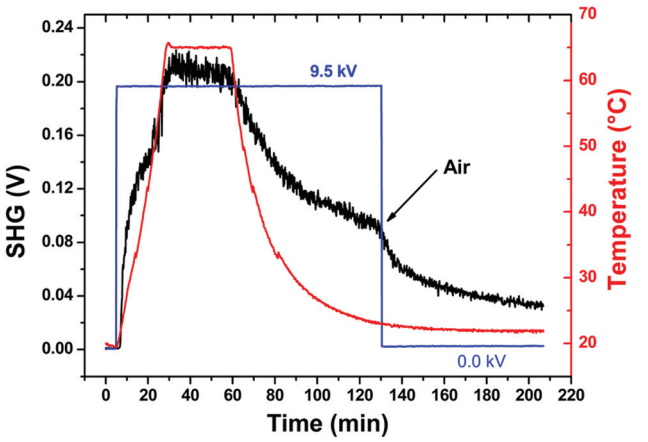

Fig. 5 *In situ* corona-wire poling dynamics of the PMMA film containing compound **3**.

No significant Stark shift of the absorption peaks was observed after poling. The second-order nonlinear optical coefficients of the poled film were obtained by the standard maker fringe technique.[26]

The coefficient values obtained for the composite PMMA film containing compound **3** are d_{31} = 0.29 pm V^{-1}, d_{15} = 0.25 pm V^{-1} and d_{33} = 0.74 pm V^{-1}. Because $d_{31} \approx d_{15}$ and since there is no appreciable absorption at 532 nm for the composite film of compound **3**, Kleinman's symmetry can be considered satisfactory.[27] Moreover, d_{33}/d_{31} and d_{33}/d_{15} are about equal to 3, suggesting that the first hyperpolarizability tensor of the chromophore is mono-dimensional. The d_{33} value is comparable with the one obtained for a ruthenium σ-alkynyl complex (0.7 pm V^{-1}), defined as remarkable.[14h]

Conclusions

In this work, novel Y-shaped ferrocene conjugated imidazole chromophores were prepared and well characterized. In addition, the HOMO–LUMO energy gaps of the chromophores were obtained from cyclic voltammetry and UV-visible experiments. These values are correlated with DFT studies. The chromophores are characterized by remarkably high $\mu\beta_{\mathrm{EFISH}}$ values in $CHCl_3$ solution and an excellent thermal stability. They are excellent candidates for SHG polymeric films, as evidenced by the interesting d_{33} value of the host/guest system based on chromophore **3** in PMMA. Finally, it is important to underline the ease with which the films for SHG measurements can be prepared; in fact the complex/matrix system is simply spin-coated on a support at room temperature.

Experimental

Materials and procedures

(1*E*,5*E*)-1,6-bisferrocenyl-hexa-1,5-diene-3,4-dione was synthesized according to the reporting procedure.[13b,14f] The pro-

ducts were dried overnight before characterization. Chromatographic purification and separation were carried out using silica gel 60 (AVRA, 100–120 mesh), hexane and ethyl acetate as solvents. All other chemicals were purchased from Sigma Aldrich Chemical Co. Imidazole derivatives were synthesized by the Debus–Radziszewski condensation reaction with (1*E*,5*E*)-1,6-bisferrocenyl-hexa-1,5-diene-3,4-dione and *para*-substituted benzaldehyde (R = H, OCH_3, CF_3, CN and NO_2) in the presence of ammonium acetate and acetic acid to form Y-shaped imidazole chromophore derivatives (**1–5**) as shown in Scheme 1.

General physical measurements

NMR spectra were recorded on a BRUKER (400 MHz) spectrometer. Chemical shifts are reported in δ (ppm) and mass spectra were recorded on a high-resolution JEOL mass spectrometer using the Electron ionization (EI) method. FT-IR spectra were obtained using a SHIMADZU IR Affinity-1 instrument equipped with a high-sensitivity DLATGS detector; the spectra were recorded as KBr discs. Electronic absorption spectra were recorded in dichloromethane, in a 1 cm^2 quartz cuvette at room temperature, using a JASCO V-670 UV-Visible spectrophotometer. Electrochemical measurements were recorded using a CHI620E electrochemical analyser; they were performed in 5×10^{-3} M solutions of dichloromethane with 0.1 M tetrabutylammonium perchlorate (TBAP, Aldrich) as the supporting electrolyte at a scan rate of 100 mV s^{-1}. A platinum wire acts as the counter electrode, glassy carbon acts as the working electrode and an Ag/AgCl electrode acts as the reference electrode. Thermogravimetric analyses were carried out using a TGA SDT Q600 V20.9 Build 20 instrument under a nitrogen atmosphere at a heating rate 20 °C min^{-1} (0–800 °C).

Synthesis of Y-shaped imidazole derivatives 1–5

Compound 1 (H). Benzaldehyde, (1 mmol), yield 65%. $C_{33}H_{28}Fe_2N_2$: calcd C, 70.24; H, 5.00; N, 4.96; found C, 69.87, H, 5.01, N, 4.90. HRMS (EI): exact mass: 564.0951, found mass: 564.0948. ^{1}H NMR (400 MHz, DMSO-d_6) δ (ppm): 12.22 (s, 1 H), 8.09 (d, J = 7.4 Hz, 2 H), 7.48 (t, J = 7.5 Hz, 2 H), 7.38 (t, J = 7.3 Hz, 1 H), 7.04 (d, J = 16 Hz, 2 H), 6.9 (d, J = 16 Hz, 2 H), 4.63 (s, 4 H), 4.30 (d, J = 19.4 Hz, 4 H), 4.13 (d, J = 15.8 Hz, 10 H). ^{13}C NMR (100 MHz, DMSO-d_6) δ (ppm): 146.84, 138.50, 130.69, 129.12, 125.94, 124.85, 117.50, 112.97, 84.78, 84.37, 69.47, 66.95. FT-IR: 3446(s), 3085(s), 2918(s), 2839(s), 1733(m), 1641(m), 1559(w), 1494(m), 1470(s), 1405(s), 1316(w), 1255(m), 1156(w), 1105(s), 1035(s), 1006(s), 924(s), 824(s), 770(m), 695(s), 657(m), 492(s) cm^{-1}. UV-visible (CH_2Cl_2, nm): 234, 367, 469.

Compound 2 (OCH_3). 4-Methoxybenzaldehyde, (1 mmol), yield 30%. $C_{34}H_{30}Fe_2N_2O$: calcd C, 68.71; H, 5.09; N, 4.71; found C, 68.57; H, 4.91, N, 4.50. HRMS (EI): exact mass: 594.1057, found mass: 594.1102. ^{1}H NMR (400 MHz, DMSO-d_6) δ (ppm): 12.09 (s, 1 H), 8.04 (d, J = 8.5 Hz, 2 H), 7.05 (d, J = 8.6 Hz, 2 H), 6.92 (d, J = 12.8 Hz, 4 H), 4.64 (s, 4 H), 4.31 (s, 4 H), 4.14 (s, 10 H), 3.83 (s, 3 H). ^{13}C NMR (100 MHz, DMSO-d_6) δ (ppm): 159.89, 146.86, 138.12, 128.05, 127.33, 124.32, 123.23, 117.41, 114.35, 112.91, 84.49, 84.34, 69.27, 66.68, 55.54. FT-IR: 3427(s), 3092(s), 2924(s), 2825(m), 1605(s), 1583(m), 1526(s), 1491(s), 1441(s), 1409(m), 1298(m), 1248(s), 1177(s), 1099(s), 1020(s), 992(s), 942(s), 820(s), 735(m), 663(m), 603(m), 497(s) cm^{-1}. UV-visible (CH_2Cl_2, nm): 234, 370, 460.

Compound 3 (CF_3). 4-Trifluoromethylbenzaldehyde, (1 mmol), yield 25%. HRMS (EI): exact mass: 632.0825, found mass: 632.0814. ^{1}H NMR (400 MHz, DMSO-d_6) δ (ppm): 12.50 (s, 1 H), 8.33 (d, J = 7.9 Hz, 2 H), 7.86 (d, J = 8.2 Hz, 2 H), 7.01 (d, J = 12 Hz, 2 H), 6.92 (d, J = 8 Hz, 2 H), 4.65 (s, 4 H), 4.30 (d, J = 23.3 Hz, 4 H), 4.17 (d, J = 19.0 Hz, 10 H). ^{19}F NMR (377 MHz, DMSO(d_6)): δ −60.87 (s, CF3). ^{13}C NMR (100 MHz, DMSO-d_6) δ (ppm): 145.23, 139.01, 134.25, 129.43, 128.72, 126.29, 125.84, 123.47, 117.18, 112.71, 84.56, 84.08, 69.50, 67.05. FT-IR: 3438(s), 3089(m), 3025(w), 1609(s), 1534(w), 1448(s), 1320(s), 1234(w), 1162(s), 1127(s), 1070(s), 1006(m), 956(s), 856(s), 820(s), 678(m), 599(w), 496(s) cm^{-1}. UV-visible (CH_2Cl_2, nm): 233, 369, 460.

Compound 4 (CN). 4-Cyanobenzaldehyde, (1 mmol), yield 47%. $C_{34}H_{27}Fe_2N_3$: calcd C, 69.30; H, 4.62; N, 7.13; found C, 70.02; H, 4.40, N, 6.90. HRMS (EI): exact mass: 589.0904, found mass: 589.0914. ^{1}H NMR (400 MHz, DMSO-d_6) δ (ppm): 12.44 (s, 1 H), 8.19 (d, J = 8.1 Hz, 2 H), 7.88 (d, J = 8.1 Hz, 2 H), 7.10, (d, J = 12 Hz, 2H), 7.01 (d, J = 12 Hz, 2 H), 4.59 (s, 4 H), 4.24 (d, J = 23.2 Hz, 4 H), 4.07 (d, J = 17.2 Hz, 10 H). ^{13}C NMR (100 MHz, DMSO-d_6) δ (ppm): 144.91, 139.26, 134.48, 133.20, 129.74, 126.24, 125.69, 119.43, 117.05, 112.57, 110.51, 84.47, 83.98, 69.51, 67.10. FT-IR: 3425(s), 3091(m), 2930(w), 2217(s), 1634(m), 1606(s), 1523(m), 1405(m), 1284(m), 1241(m), 1177(m), 1113(s), 1049(m), 1006(m), 952(s), 824(s), 735(m), 556(s), 492(s) cm^{-1}. UV-visible (CH_2Cl_2, nm): 234, 370, 438.

Compound 5 (NO_2). 4-Nitrobenzaldehyde, (1 mmol), yield 25%. $C_{33}H_{27}Fe_2N_3O_2$: calcd C, 65.05; H, 4.47; N, 6.90; found C, 65.12; H, 4.04; N, 6.68. HRMS (EI): exact mass: 609.2880, found mass: 609.2908. ^{1}H NMR (400 MHz, DMSO-d_6) δ (ppm): 12.62 (s, 1 H), 8.38 (d, J = 8 Hz, 2 H), 8.34 (d, J = 8 Hz, 2 H), 7.10 (m, 4 H), 4.69 (d, J = 8, 4 H), 4.38 (d, J = 24 Hz, 4 H), 4.18 (d, J = 16 Hz, 10 H). ^{13}C NMR (100 MHz, DMSO-d_6) δ (ppm): 146.94, 144.58, 139.64, 136.25, 130.22, 126.79, 126.00, 124.72, 116.91, 112.98, 84.36, 83.86, 69.50, 67.18. FT-IR: 3385(m), 3092(m), 2929(m), 2860(w), 1626(w), 1605(s), 1519(s), 1387(m), 1344(s), 1237(w), 1184(w), 1099(s), 1038(w). 998(s), 949(m), 856(s), 813(s), 753(w), 692(s), 485(s) cm^{-1}. UV-visible (CH_2Cl_2, nm): 235, 372, 480.

Single-crystal X-ray structure determination of compound 4

Red crystals of compound **4** were obtained by slow evaporation of the corresponding solution of methanol at room temperature. The crystal was stored in paraffin-oil and mounted in a MiTeGenloop, and measured at 298 K. The approximate dimensions of the crystal are $0.32 \times 0.25 \times 0.16$ mm^3. The X-ray diffraction data were recorded using a Bruker Kappa Apex II coupled with a CCD area detector and a graphite diffractometer with Mo-Kα radiation (λ = 0.71073 Å). The Apex2 (ref. 28) package was used for cell refinements and data reduction. The structure was solved by direct methods using the SHELXS-97

(ref. 29) or Superflip[30] program with the OLEX2 (ref. 31) graphical user interface. Structural refinements were carried out using Shelxl-2018.[32] The crystallographic details are summarized in Table S1.†

Computational calculation methods

The electronic structures and molecular properties of ferrocene conjugated Y-shaped imidazole chromophores were investigated using density functional theory (DFT) for understanding the bonding patterns, electronic charges and molecular orbital energy distributions. The initial geometry of the chromophore was taken from the available crystal data for compound **4**. The remaining chromophores were obtained by replacing the **CN** substituent of compound **4** with a suitable R substituent (see Scheme 1). The geometries of the synthesized chromophores in the gas phase were optimized using Becke's three-parameter and the Lee–Yang–Parr functional as B3LYP.[19] Computational calculations at the B3LYP level were carried out using the 6-31+G** basis set for finding the global minimum energy structures of all chromophores and their molecular properties. All computation calculations were performed using the G09 package[33] and the frontier molecular orbital density plots were visualized using the GaussView 5.0 (ref. 34) program.

EFISH measurements

All the Y-shaped imidazole chromophores were studied by EFISH[21] in $CHCl_3$ solutions at 10^{-3} M concentration, with a non-resonant incident wavelength of 1907 nm, obtained by Raman-shifting the fundamental 1064 nm wavelength using a Q-switched, mode-locked Nd^{3+}:YAG laser manufactured by Atalaser. The apparatus used for EFISH measurements is a proto type made by SOPRA (France). The values of $\mu\beta_{EFISH}$ reported are the mean values of 16 measurements performed on the same sample. The sign of $\mu\beta$ is determined by comparison with the reference solvent ($CHCl_3$).

Preparation of thin films of chromophore 3 in PMMA

The composite film was prepared by spin coating on ordinary non-pretreated glass substrates (thickness 1 mm) cleaned with water/acetone. The solution was obtained from 300 mg of polymethylmethacrylate (PMMA) and 15 mg of compound **3** dissolved in dichloromethane (4.5 mL). The parameters of spinning (RPM-revolutions per minute) are RPM 1: 500; Ramp 1: 1 s, Time 1: 3 s; RPM 2: 1500; Ramp 2: 4 s, Time 2: 25 s; RPM 3: 2000; Ramp 3: 1 s, Time 3: 1 s. The film thickness of composite PMMA/compound **3** was measured by using a profilometer. Second Harmonic Generation (SHG) experiments were performed using a Q-switched Nd:YAG (Quanta System Giant G790-20) laser at a 1.064 μm wavelength with a pulse of 7 ns and a repetition rate of 20 Hz. For poling measurements, the fundamental beam was attenuated to 0.57 mJ and was focused with a lens (f = 600 mm) on the sample, placed over the hot stage. The corona poling process was carried out inside a specially built dry box, in a N_2 atmosphere. The fundamental beam was polarized in the plane of incidence (p-polarized) with an angle of about 55° with respect to the sample in order to optimize the SHG signal. The hot stage temperature was controlled by using a GEFRAN 800 controller, while the corona wire voltage (up to 10.0 kV across a 10 mm gap) was applied by using a TREK610E high-voltage-supplier. After rejection of the fundamental beam by using an interference filter and a glass cut-off filter, a p-polarized SHG signal at 532 nm was detected with a UV-vis photomultiplier (PT) Hamamatsu C3830.[14f,35] The corona wire poling dynamics of the SHG behaviour of the PMMA composite film was investigated at 65 °C in a N_2 atmosphere with an electric field of 9.5 kV; these conditions allowed us to obtain a sufficiently high and stable second-harmonic generation (SHG) signal. The absorption bands of compound **3** in the PMMA film (peak at 370 nm) after poling (red lines) decrease compared to those observed before poling (blue lines). It is the so-called "dichroic effect"[25a] due to the partial orientation of the molecules along the direction of the electric poling field. No appreciable Stark shift[25a] of the absorption peaks was observed after poling as shown in Fig. S1.†

Method of determination of the d_{33} values

In the Maker fringe experiment, the second harmonic (SH) intensity was detected as a function of the incidence angle θ of the normalized and fundamental beam with respect to that of a calibrated quartz crystal wafer (X-cut) 1.15 mm in thickness whose d_{11} is 0.46 pm V^{-1}. The incidence angle was changed by rotating the poled film along the Y-axis while the polarization of the fundamental and SH beam could be changed by a half-wave plate and a cube beam splitter respectively. In order to determine the nonzero independent components of the susceptibility tensor for the poled film ($C \infty v$ symmetry) Maker fringe measurements were performed with the following polarizations: p → p, s → p and 45 → s. The standard expression[26] used to fit the SHG intensity in the Maker fringe measurement includes the absorption coefficient of the film at the harmonic frequency. In this expression the SHG intensity is proportional to the square of the effective nonlinear optical coefficient (d_{eff}) which depends on the polarizations of the fundamental and SH beam. Considering the $C \infty v$ symmetry expected for the poled film and the polarizations of the fundamental and SH beam, the coefficient d_{eff} assumes the following expression:

$$d_{\text{eff}} = d_{zxx} \sin \vartheta 2 \tag{1a}$$

For s → p configuration,

$$d_{\text{eff}} = d_{xxz} \sin \vartheta 1 \tag{1b}$$

For 45 → s configuration,

$$d_{eff} = 2d_{xxz} \sin \vartheta 1 \cos \vartheta 1 \cos \vartheta 2 + \sin \vartheta 2 (d_{zxx} \cos 2\vartheta 1 + d_{zzz} \sin 2\vartheta 1) \tag{1c}$$

for p → p configuration,where $\theta 1$ and $\theta 2$ are the angles of refraction inside the poled film for the fundamental and SH beam with refractive indices $n\omega$ and $n2\omega$ ($\sin \theta m = \sin \theta / nm\omega$, m = 1,2), respectively.

Conflicts of interest

There are no conflicts to declare.

Acknowledgements

We gratefully acknowledge the financial support from the DST Indo-Italian Joint Project (no. INT/Italy/P-15/2016(SP). The "Ministero degli Affari Esteri e della Cooperazione Internazionale" is also acknowledged (bilateral project Italy-India, Prot. no. MAE0065640) for financial support. The authors gratefully acknowledge VIT-SIF for providing instrumental facilities. We are very grateful to STIC-India, Cochin for providing single-crystal XRD data.

Notes and references

1 (*a*) J. Zyss, *Molecular Nonlinear Optics: Materials, Physics and Devices*, Academic Press, Boston, 1994; (*b*) N. P. Prasad and D. J. Williams, *Introduction to Nonlinear Optical Effects in molecules and Polymers*, Wiley, 1991; (*c*) B. E. Urban, P. Neogi, K. Senthilkumar, S. K. Rajpurhit, P. Jagadeeshwaran, S. Kim, Y. Fujita and A. Neogi, *IEEE J. Sel. Top. Quantum Electron.*, 2012, **18**(4), 1451–1456.

2 (*a*) W. Chen, T. Salim, H. Fan, L. James, Y. M. Lam and Q. Zhang, *RSC Adv.*, 2014, **4**, 25291–25301; (*b*) L. Beverina, R. Ruffo, G. Patriarca, F. De Angelis, D. Roberto, S. Righetto, R. Ugo and G. A. Pagani, *J. Mater. Chem.*, 2009, **19**, 8190–8197; (*c*) C. Y. Jung, C. J. Song, W. Yao, J. M. Park, I. H. Hyun, D. H. Seong and J. Y. Jaung, *Dyes Pigm.*, 2015, **121**, 204–210; (*d*) K. Pei, Y. Wu, H. Li, Z. Geng, H. Tian and W.-H. Zhu, *ACS Appl. Mater. Interfaces*, 2015, **7**, 5296–5304.

3 (*a*) F. Bures, H. Cermakova, J. Kulhanek, M. Ludwig, W. Kuznik, I. V. Kityk, T. Mikysek and A. Ruzicka, *Eur. J. Org. Chem.*, 2012, 529–538; (*b*) K. Pei, Y. Wu, A. Islam, S. Zhu, L. Han, Z. Geng and W. Zhu, *J. Phys. Chem. C*, 2014, **118**, 16552–16561.

4 (*a*) M. Klikar, P. Solanke, J. Tydlitat and F. Bures, *Chem. Rec.*, 2016, **16**(4), 1886–1905; (*b*) M. Pokladko-Kowar, N. Nosidlak, E. Gondek, I. V. Kityk, F. Bures, J. Kulhanek and P. Karasinski, *Opt. Quantum Electron.*, 2016, **48**, 82–91; (*c*) P. Solanke, F. Bures, O. Pytela, M. Klikar, T. Mikysek, L. Mager, A. Barsella and Z. Ruzickova, *Eur. J. Org. Chem.*, 2015, 5339–5349.

5 (*a*) J. E. Kwon, S. Park and S. Y. Park, *J. Am. Chem. Soc.*, 2013, **135**, 11239–11246; (*b*) K. Feng, L. D. Boni, L. Misoguti, C. R. Mendonca, M. Meador, F. L. Hsud and X. R. Bu, *Chem. Commun.*, 2004, **10**, 1178–1180; (*c*) G. Qian and Z. Y. Wang, *Chem. – Asian J.*, 2010, **5**, 1006–1029; (*d*) R. Chauhan, M. Shahid, M. Trivedi, D. P. Amalnerkar and A. Kumar, *Eur. J. Inorg. Chem.*, 2015, **22**, 3700–3707; (*e*) C. Duan, F. Huang and Y. Cao, *J. Mater. Chem. C*, 2012, **22**, 10416–10434; (*f*) B. Walker, C. Kim and T. Q. Nguyen, *Chem. Mater.*, 2011, **23**, 470–482.

6 (*a*) I. D. L. Albert, T. J. Marks and M. A. Ratner, *J. Am. Chem. Soc.*, 1997, **119**, 6575–6582; (*b*) S. Di Bella, *Chem. Soc. Rev.*, 2001, **30**, 355–366; (*c*) F. Tessore, D. Roberto, R. Ugo, P. Mussini, S. Quici, I. Ledoux-Rak and J. Zyss, *Angew. Chem., Int. Ed.*, 2003, **42**, 456–459; (*d*) E. Rossi, A. Colombo, C. Dragonetti, S. Righetto, D. Roberto, R. Ugo, A. Valore, J. A. G. Williams, M. G. Lobello, F. De Angelis, S. Fantacci, I. Ledoux-Rak, A. Singh and J. Zyss, *Chem. – Eur. J.*, 2013, **19**, 9875–9883; (*e*) A. Valore, M. Balordi, A. Colombo, C. Dragonetti, S. Righetto, D. Roberto, R. Ugo, T. Benincori, G. Rampinini, F. Sannicolò and F. Demartin, *Dalton Trans.*, 2010, **39**, 10314–10318; (*f*) S. Di Bella, C. Dragonetti, M. Pizzotti, D. Roberto, F. Tessore and R. Ugo, in *Topics in Organometallic Chemistry 28. Molecular Organometallic Materials for Optics*, ed. H. Le Bozec and V. Guerchais, Springer-Verlag, Berlin/Heidelberg, 2010, pp. 1–55; (*g*) J. Boixel, V. Guerchais, H. Le Bozec, A. Chantzis, D. Jacquemin, A. Colombo, C. Dragonetti, D. Marinotto and D. Roberto, *Chem. Commun.*, 2015, **51**, 7805–7808; (*h*) C. Hierlinger, D. B. Cordes, A. M. Z. Slawin, A. Colombo, C. Dragonetti, S. Righetto, D. Roberto, D. Jacquemin, E. Zysman-Colman and V. Guerchais, *Dalton Trans.*, 2018, **47**, 8292–8300; (*i*) M. Fontani, E. Garoni, A. Colombo, C. Dragonetti, S. Fantacci, H. Doucet, J. F. Soule, J. Boixel, V. Guerchais and D. Roberto, *Dalton Trans.*, 2019, **48**, 202–208.

7 (*a*) K. Y. Suponitsky, T. V. Timofeeva and M. Y. Antipin, *Russ. Chem. Rev.*, 2006, **75**, 457–496; (*b*) M. Stahelin, D. M. Burland, M. Ebert, R. D. Miller, B. A. Smith, R. J. Twieg, W. Vilksen and C. A. Walsh, *Appl. Phys. Lett.*, 1992, **61**, 1626–1628.

8 (*a*) Y. Wu and W. Zhu, *Chem. Soc. Rev.*, 2013, **42**, 2039–2058; (*b*) C. Dragonetti, M. Pizzotti, D. Roberto and S. Galli, *Inorg. Chim. Acta*, 2002, **330**, 128–135; (*c*) M. Pizzotti, R. Ugo, D. Roberto, S. Bruni, P. Fantucci and C. Rovizzi, *Organometallics*, 2002, **21**, 5830–5840.

9 (*a*) W. Wu, Z. Zhang and X. Zhang, *J. Nonlinear Opt. Phys. Mater.*, 2005, **14**, 61; (*b*) X. R. Bu, H. Li, D. Van Derveer and E. A. Mintz, *Tetrahedron Lett.*, 1996, **37**, 7331–7334; (*c*) C. G. Densmore and P. G. Rasmussen, *Macromolecules*, 2004, **37**, 5900–5910; (*d*) F. Bures, J. Kulhanek, T. Mikysek, J. Ludvik and J. Lokaj, *Tetrahedron Lett.*, 2010, **51**, 2055–2058; (*e*) J. Kulhanek, F. Bures, T. Mikysek, J. Ludvik and O. Pytela, *Dyes Pigm.*, 2011, **90**, 48–55; (*f*) J. Kulhanek and F. Bures, *Beilstein J. Org. Chem.*, 2012, **8**, 25–49.

10 (*a*) J. Ren, S. M. Wang, L. F. Wu, Z. X. Xu and B. H. Dong, *Dyes Pigm.*, 2008, **76**, 310–314; (*b*) J. Santos, E. A. Mintz, O. Zehnder, C. Bosshard, X. R. Bua and P. Gunter, *Tetrahedron Lett.*, 2001, **42**, 805–808.

11 (*a*) S. Scuppa, L. Orian, D. Dini, S. Santi and M. Meneghetti, *J. Phys. Chem. A*, 2009, **113**, 9286–9294; (*b*) M. Zaarour, A. Singh, C. Latouche, J. A. G. Williams, I. Ledoux-Rak, J. Zyss, A. Boucekkine, H. Le Bozec, V. Guerchais, C. Dragonetti, A. Colombo, D. Roberto and A. Valore, *Inorg. Chem.*, 2013, **52**, 7987–7994.

12 (*a*) M. L. Green, S. R. Marder, M. E. Thompson, J. A. Bandy, D. Bloor, P. V. Kolinsky and R. J. Jones, *Nature*, 1987, **330**, 360–362; (*b*) M. Y. Teng, J. Zhang, G. L. Huang, B. Liu, X. M. Li, M. Z. Rong, T. H. Shen and Q. B. Song, *J. Organomet. Chem.*, 2015, **791**, 298–302; (*c*) J. Mata, E. Peris, S. Uriel, R. Llusar, S. Houbrechts and A. Persoons, *Polyhedron*, 2001, **20**, 2083–2088; (*d*) S. Venkatraman, R. Kumar, J. Sankar, T. K. Chandrashekar, K. Sendhil, C. Vijayan, A. Kelling and M. O. Senge, *Chem. – Eur. J.*, 2004, **10**, 1423–1432; (*e*) I. Janowska, J. Zakrzewski, K. Nakatani, M. Palusiak, M. Walak and H. Scholl, *J. Organomet. Chem.*, 2006, **691**, 323–330; (*f*) S. Kaur, M. Kaur, P. Kaur, K. Clays and K. Singh, *Coord. Chem. Rev.*, 2017, **343**, 185–219; (*g*) D. Hadji, A. Rahmouni, D. Hammoutène and O. Zekri, *J. Mol. Liq.*, 2019, **286**, 110939; (*h*) P. Deveci, B. Taner, E. Özcan, Z. Kılıç, M. Karakaya and A. Karakas, *Russ. J. Gen. Chem.*, 2019, **89**, 330–338; (*i*) R. Teimuri-Mofrad, K. Rahimpour, R. Ghadari and S. Ahmadi-Kandjani, *J. Mol. Liq.*, 2017, **244**, 322–329.

13 (*a*) G. Sathyaraj, M. Kiruthika, T. Weyhermüller and B. U. Nair, *Organometallics*, 2012, **31**, 6980–6987; (*b*) G. Sathyaraj, D. Muthamilselvan, M. Kiruthika, T. Weyhermüller and B. U. Nair, *J. Organomet. Chem.*, 2012, **716**, 150–158.

14 (*a*) R. Macchi, E. Cariati, D. Marinotto, D. Roberto, E. Tordin, R. Ugo, R. Bozio, M. Cozzuol, D. Pedron and G. Mattei, *J. Mater. Chem.*, 2010, **20**, 1885–1890; (*b*) D. Marinotto, R. Castagna, S. Righetto, C. Dragonetti, A. Colombo, C. Bertarelli, M. Garbugli and G. Lanzani, *J. Phys. Chem. C*, 2011, **115**, 20425–20432; (*c*) A. Colombo, C. Dragonetti, D. Marinotto, S. Righetto, D. Roberto, S. Tavazzi, M. Escadeillas, V. Guerchais, H. Le Bozec, A. Boucekkine and C. Latouche, *Organometallics*, 2013, **32**, 3890–3894; (*d*) A. Colombo, C. Dragonetti, D. Marinotto, I. P. Oliveri, S. Righetto, M. G. Lobello and F. De Angelis, *Chem. Commun.*, 2014, **50**, 7986–7989; (*e*) C. Dragonetti, A. Colombo, D. Marinotto, S. Righetto, D. Roberto, A. Valore, M. Escadeillas, V. Guerchais, H. Le Bozec, A. Boucekkine and C. Latouche, *J. Organomet. Chem.*, 2014, **751**, 568–572; (*f*) K. Senthilkumar, K. Thirumoorthy, C. Dragonetti, D. Marinotto, S. Righetto, A. Colombo, M. Haukka and N. Palanisami, *Dalton Trans.*, 2016, **45**, 11939–11943; (*g*) H. Zhao, E. Garoni, T. Roisnel, A. Colombo, C. Dragonetti, D. Marinotto, S. Righetto, D. Roberto, D. Jacquemin, J. Boixel and V. Guerchais, *Inorg. Chem.*, 2018, **57**, 7051–7063; (*h*) A. Colombo, C. Dragonetti, D. Marinotto, S. Righetto, G. Griffini, S. Turri, H. Akdas-Kilig, J.-L. Fillaut, A. Amar, A. Boucekkine and C. Katan, *Dalton Trans.*, 2016, **45**, 11052–11060.

15 J. D. Dunitz, L. E. Orgel and A. Rich, *Acta Crystallogr.*, 1956, **9**, 373–375.

16 (*a*) C. Imrie, P. Kleyi, V. O. Nyamori, T. I. A. Gerber, D. C. Levendis and J. Look, *J. Organomet. Chem.*, 2007, **692**, 3443–3453; (*b*) K. Senthilkumar, M. Pizzotti, K. Thirumoorthy, G. Di Carlo, S. Righetto, A. Orbelli Biroli, M. Haukka and N. Palanisami, *J. Phys. Chem. C*, 2016, **120**, 20277–202311; (*c*) E. David, K. Thirumoorthy and N. Palanisami, *Appl. Organomet. Chem.*, 2018, **32**, e4522.

17 N. G. Connelly and W. E. Geiger, *Chem. Rev.*, 1996, **96**, 877–910.

18 M. Zaheer, A. Shah, Z. Akhter, R. Qureshi, B. Mirza, M. Tauseef and M. Bolte, *Appl. Organomet. Chem.*, 2011, **25**, 61–69.

19 (*a*) R. L. Martin, *J. Chem. Phys.*, 2003, **118**, 4775–4777; (*b*) C. Lee, W. Yang and R. G. Parr, *Phys. Rev. B: Condens. Matter Mater. Phys.*, 1988, **37**, 785–789; (*c*) R. G. Parr and Y. Weitao, *Density-Functional Theory of Atoms and Molecules*, Oxford University Press, Oxford, 1994; (*d*) S. H. Vosko, L. Wilk and M. Nusair, *Can. J. Phys.*, 1980, **58**, 1200–1211.

20 (*a*) Y. Zhang, S. L. Lai, Q. W. Tong, M. F. Lo, T. W. Ng, M. Y. Chan, Z. C. Wen, J. He, K. S. Jeff, X. L. Tang, W. M. Liu, C. C. Ko, P. F. Wang and C. S. Lee, *Chem. Mater.*, 2011, **24**, 61–70; (*b*) J. Jayabharathi, V. Thanikachalam and M. V. Perumal, *Spectrochim. Acta, Part A*, 2012, **92**, 113–121.

21 (*a*) B. F. Levine and C. G. Bethea, *J. Chem. Phys.*, 1975, **63**, 2666–2682; (*b*) I. Ledoux and J. Zyss, *J. Chem. Phys.*, 1982, **73**, 203–213.

22 (*a*) P. D. Maker, *Phys. Rev. A: At., Mol., Opt. Phys.*, 1970, **1**, 923–951; (*b*) K. Clays and A. Persoons, *Phys. Rev. Lett.*, 1991, **66**, 2980–2983; (*c*) J. Zyss and I. Ledoux, *Chem. Rev.*, 1994, **94**, 77–105.

23 (*a*) M. R. S. A. Janjua, Z. M. Su, W. Guan, C. G. Liu, L. K. Yan, P. Song and G. Maheen, *Aust. J. Chem.*, 2010, **63**, 836–844; (*b*) M. G. Vivas, D. L. Silva, J. Malinge, M. Boujtita, R. Zalesny, W. Bartkowiak, H. Agren, S. Canuto, L. De Boni, E. Ishow and C. R. Mendonca, *Sci. Rep.*, 2014, **4**, 4447; (*c*) H. Xu, Y. Yue, H. Wang, L. Chen, Y. Hao and B. Xu, *J. Lumin.*, 2012, **132**, 919–923.

24 (*a*) M. R. S. A. Janjua, W. Guan, L. Yan, Z. M. Su, A. Karim and J. Akbar, *Eur. J. Inorg. Chem.*, 2010, **22**, 3466–3472; (*b*) G. Hennrich, M. T. Murillo, P. Prados, H. Al-Saraierh, A. El-Dali, D. W. Thompson, J. Collins, P. E. Georghiou, A. Teshome, I. Asselberghs and K. Clays, *Chem. – Eur. J.*, 2001, **13**, 7753–7761.

25 (*a*) R. H. Page, M. C. Jurich, B. Beck, A. Sen, R. J. Twieg, J. D. Swalen, G. C. Bjorklund and C. G. Wilson, *J. Opt. Soc. Am. B*, 1990, **7**, 1239–1250; (*b*) M. A. Mortazavi, A. Knoesen, S. T. Kowel, B. G. Higgins and A. Dienes, *J. Opt. Soc. Am. B*, 1989, **6**, 733–741.

26 W. N. Herman and L. M. Hayden, *J. Opt. Soc. Am. B*, 1995, **12**, 416–427.

27 D. A. Kleinman, *Phys. Rev.*, 1962, **126**, 1977–1979.

28 A. X. S. Bruker, *APEX2-Software Suite for Crystallographic Programs*, Bruker AXS Inc., Madison, 2009.

29 G. M. Sheldrrick, *Acta Crystallogr., Sect. A: Found. Crystallogr.*, 2008, **64**, 112–122.

30 L. Palatinus and G. Chapuis, *J. Appl. Crystallogr.*, 2007, **40**, 786–790.

31 O. V. Dolomanov, L. J. Bourhis, R. J. Gildea, J. A. K. Howard and H. Puschmann, *J. Appl. Crystallogr.*, 2009, **42**, 339–341.

32 G. M. Sheldrick, *SHELXTL Version 2018/3*, http://shelx.uni-ac.gwdg.de/SHELX/index.php.

33 M. J. Frisch, G. W. Trucks, H. B. Schlegel, G. E. Scuseria, M. A. Robb, J. R. Cheeseman, G. Scalmani, V. Barone, B. Mennucci, G. A. Petersson, H. Nakatsuji, M. Caricato, X. Li, H. P. Hratchian, A. F. Izmaylov, J. Bloino, G. Zheng, J. L. Sonnenberg, M. Hada, M. Ehara, K. Toyota, R. Fukuda, J. Hasegawa, M. Ishida, T. Nakajima, Y. Honda, O. Kitao, H. Nakai, T. Vreven, J. A. Montgomery Jr., J. E. Peralta, F. Ogliaro, M. Bearpark, J. J. Heyd, E. Brothers, K. N. Kudin, V. N. Staroverov, R. Kobayashi, J. Normand, K. Raghavachari, A. Rendell, J. C. Burant, S. S. Iyengar, J. Tomasi, M. Cossi, N. Rega, J. M. Millam, M. Klene, J. E. Knox, J. B. Cross, V. Bakken, C. Adamo, J. Jaramillo, R. Gomperts, R. E. Stratmann, O. Yazyev, A. J. Austin, R. Cammi, C. Pomelli, J. W. Ochterski, R. L. Martin, K. Morokuma, V. G. Zakrzewski, G. A. Voth, P. Salvador, J. J. Dannenberg, S. Dapprich, A. D. Daniels, Ö. Farkas, J. B. Foresman, J. V. Ortiz, J. Cioslowski and D. J. Fox, *Gaussian09 Rev. C.01*, Gaussian, Inc., Wallingford, CT, 2009.

34 R. Dennington, T. Keith and J. Millam, *GaussView, Version 5.0.9*, Semichem Inc., Shawnee Mission, KS, 2009.

35 (*a*) D. Marinotto, S. Proutiere, C. Dragonetti, A. Colombo, P. Ferruti, D. Pedron, M. C. Ubaldi and S. Pietralunga, *J. Non-Cryst. Solids*, 2011, **357**, 2075–2080; (*b*) S. Proutiere, P. Ferruti, R. Ugo, A. Abbotto, R. Bozio, M. Cozzuol, C. Dragonetti, E. Emilitri, D. Locatelli, D. Marinotto, G. Pagani, D. Pedron and D. Roberto, *Mater. Sci. Eng., B*, 2008, **147**, 293–297.